Organic Geochemistry 196 (2024) 104840

Contents lists available at ScienceDirect

Organic Geochemistry

journal homepage: www.elsevier.com/locate/orggeochem

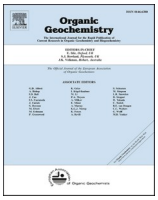

Large variability and ^{2}H-depletion of Middle Miocene to Pleistocene alkenone hydrogen isotopes in the Equatorial Pacific reflect subsurface, low light haptophyte growth

Katrin Hättig [a,*], Panteleimon Prokopiou [a,1], Stefan Schouten [a,b], Marcel T.J. van der Meer [a]

[a] Department of Marine Microbiology and Biogeochemistry, NIOZ Royal Netherlands Institute for Sea Research, Texel, the Netherlands
[b] Department of Earth Sciences, Faculty of Geosciences, Utrecht University, Utrecht, the Netherlands

ARTICLE INFO

Associate Editor – Kliti Grice

Keywords:
Alkenones
Hydrogen isotopes
Carbon isotopes
Equatorial Pacific

ABSTRACT

Hydrogen isotope ratios of haptophyte derived long-chain alkenones ($\delta^{2}H_{C37:2}$) have shown to be a useful tool for reconstructing past isotopic compositions of surface seawater ($\delta^{2}H_{SSW}$). The $\delta^{2}H_{SSW}$ is related to global ice volume, sea surface salinity and the local hydrological cycle. Here, we present a hydrogen isotope record of alkenones spanning the last 14.5 Ma from IODP site U1338 in the east equatorial Pacific. The alkenone-based reconstructed $\delta^{2}H_{SSW}$ is substantially more negative and variable than reconstructed $\delta^{2}H_{SSW}$ based on published oxygen isotopes of coccolith carbonates. This suggests that factors other than the isotopic composition of seawater affect the hydrogen isotopic composition of alkenones. The relatively negative and highly variable $\delta^{2}H_{C37:2}$ values are in line with published modern observations on alkenones from suspended particulate matter in the equatorial and north Pacific, with the highest values at relatively high light conditions at the surface and the lowest values at higher water depth and relatively low light conditions. This suggests that the relatively negative and highly variable $\delta^{2}H_{C37:2}$ values in these Middle Miocene to Pleistocene sediments are likely derived from haptophytes growing below the sea surface under variable low light conditions. In regions where the contribution of alkenones from subsurface production, due to high subsurface nutrients, at low light intensities to the sediment is relatively high the $\delta^{2}H_{C37:2}$ has to be interpreted with care as a proxy for $\delta^{2}H_{SSW}$.

1. Introduction

Between the Middle Miocene and Pleistocene, the Earth experienced a climate transition from a warm period towards a modern 'ice-house' climate with growth of the Antarctic Ice sheet (ca. 13.9 Ma) (Flower and Kennett, 1994) and emerging large Northern Hemisphere Glaciations (NHG) (ca. 3 Ma) (Mudelsee and Raymo, 2005; Lawrence et al., 2006). Tectonic changes such as the gradual closure of the Central American Seaway (CAS) and isolation of the Atlantic Ocean and Caribbean Sea from the Pacific Ocean (Haug et al., 2001; Steph et al., 2006; Kamikuri et al., 2009) and the narrowing Indonesian seaway (Haug and Tiedemann, 1998; Srinivasan and Sinha, 2000) led to the establishment of East-West atmospheric and oceanographic patterns across the Pacific. The eastern equatorial Pacific is therefore an interesting site to study changes in oceanography and global ice volume related to climate change from Miocene to the Pleistocene (e.g., Herbert et al., 2016; Rousselle et al., 2013; Pälike et al., 2010; Pälike et al., 2009). A continuous high-resolution 20 million years long benthic foraminiferal oxygen isotope record ($\delta^{18}O_{benthic}$) of IODP site U1337 in the eastern equatorial Pacific (Tian et al., 2013, 2014, 2018; Holbourn et al., 2015) shows a long-term decrease in deep Pacific Ocean temperature and, possibly, increase in global ice volume (Fig. 1, S1). The Pacific surface ocean has cooled by ~6–7 °C during the same period as evidenced in the $U^{K'}_{37}$ temperature record of ODP Site 846 (Fig. 1, S1; Liu and Herbert, 2004; Lawrence et al., 2006; Herbert et al., 2016) and IODP Site U1338 (Fig. 1, S1; Rousselle et al., 2013; Beltran et al., 2019). The cooling of the surface ocean displays a similar long-term trend and glacial/interglacial cycles as the $\delta^{18}O_{benthic}$ record (Tian et al., 2018). The equatorial Pacific benthic foraminiferal carbon isotope record ($\delta^{13}C_{benthic}$) (Fig. S1; Tian et al., 2013, 2014, 2018) shows a long-term decrease which is mainly controlled by continental chemical weathering and changes in the ocean circulation, e.g., with the formation of the Isthmus of Panama (between

* Corresponding author.
E-mail addresses: katrin.haettig@nioz.nl, katrin.haettig@rub.de (K. Hättig).
[1] Present address: Organic Geochemistry Unit, School of Chemistry, University of Bristol, Cantock's Close, Bristol, UK.

https://doi.org/10.1016/j.orggeochem.2024.104840
Received 8 March 2024; Received in revised form 10 June 2024; Accepted 17 July 2024
Available online 23 July 2024

12.1–9.2 Ma). From 12.1 Ma the inorganic carbon isotope record has become more negative in the Pacific than in the Atlantic Ocean (Tian et al., 2018). Although much is known with respect to the evolution of seawater temperature and oceanographic patterns in the Pacific during the Miocene and Pliocene, less is clear on the evolution of sea surface salinity. Generally, this is inferred from oxygen isotopes of calcite shells but these reflect not only the isotopic composition of seawater ($\delta^{18}O_{SW}$), a proxy for salinity, but also the temperature of seawater (e.g., Shackleton, 1974; Savin et al., 1975) making it challenging to disentangle the signals. A variety of different corrections and temperature proxies (e.g., TEX_{86}, $U^{K'}_{37}$, Mg/Ca, carbonate clumped isotopes) have been used to infer $\delta^{18}O_{SW}$ from oxygen isotopes of calcite shells from the Pacific Ocean (Beltran et al., 2007; Lear et al., 2000; Rousselle et al., 2013; Hättig et al., 2023). Furthermore, most records are from benthic foraminifera and thus only indicate the evolution of bottom water oxygen isotopes rather than surface waters.The hydrogen isotope ratio of alkenones (δ^2H_{C37}), compounds derived from haptophyte algae (Volkman et al., 1980; de Leeuw et al., 1980), has been proposed and applied as a proxy to reconstruct salinity (e.g., Schouten et al., 2006; Pahnke et al., 2007; van der Meer et al., 2007; Sangiorgi et al., 2008; Leduc et al., 2013; Kasper et al., 2014) and/or reconstructing seawater isotope ratios (e.g., Gould et al., 2019; Mitsunaga et al., 2022; Hättig et al., 2023; 2024a). Unlike oxygen isotopes of foraminifera, hydrogen isotopes of alkenones show no relationship with temperature (Schouten et al., 2006). Culture studies have shown that the fractionation of hydrogen of C_{37} alkenones is dependent on light intensity, nutrient availability and growth rate (e.g., Schouten et al., 2006; Wolhowe et al., 2009; M'Boule et al., 2014; van der Meer et al., 2015) and a large effect of haptophyte species, coastal versus oceanic, has been observed on the fractionation factor of hydrogen isotopes (Chivall et al., 2014; M'Boule et al., 2014; Sachs et al., 2016). However, these factors are generally thought to be of limited importance in modern settings, as the same species are typically dominant in open marine environments (*E. huxleyi* or *G. oceanica*) and light and nutrient conditions are optimal during the periods of algal blooms, when most of the alkenones reaching the sediment are likely being produced. Indeed, the strong relationship between δ^2H_{C37} and hydrogen isotopic composition of seawater (δ^2H_{SW}) observed in marine environmental samples suggest that ecological factors, such as growth rate and light (e.g., Wolhowe et al., 2009; Chivall et al., 2014; Sachs and Kawka, 2015; van der Meer et al., 2015; Sachs et al., 2017; Weiss et al., 2017) might be less important than the hydrogen isotopic composition of seawater (Gould et al., 2019; Mitsunaga et al., 2022).

Here we reconstructed the hydrogen isotopic composition of surface seawater (δ^2H_{SSW}) for the east equatorial Pacific during the Middle Miocene to Pleistocene by generating a hydrogen isotope record of $C_{37:2}$ alkenones ($\delta^2H_{C37:2}$) of IODP site U1338. Uniquely, we can compare this to a record of surface seawater oxygen isotopes ($\delta^{18}O_{SSW}$) reconstructed from previously published oxygen isotopes of coccolith carbonate and $U^{K'}_{37}$ sea surface temperature, also derived from haptophyte algae (Rousselle et al., 2013). This allows to compare two independent proxies for surface seawater isotopes, derived from the same group of organisms, during this climatically important period.

2. Material and methods

2.1. Geographic Setting

The Integrated Ocean Drilling Program (IODP) drilling site U1338 is located at coordinates 2°30.469′N, 117°58.178′W, with a water depth of 4200 m (IODP 'PEAT' Expedition 32, Pälike et al., 2010; Pälike et al., 2009). The sediments were deposited above the calcite compensation depth on an 18 million year old crust and within the equatorial zone (within ±2° of the equator) during the Miocene and Pleistocene periods (Pälike et al., 2010). Today, the core is located within the modern eastern cold tongue in the equatorial Pacific (Fig. 1). The complex oceanic circulation in the eastern Pacific is primarily influenced by the Walker cell circulation and trade winds (Cannariato and Ravelo, 1997; Kamikuri et al., 2009). The South and North Equatorial currents (SEC and NEC) move from East to West, causing warm waters to accumulate in the West Pacific Warm Pool (WPWP). This creates a pressure gradient, leading to the Equatorial Undercurrent (EUC) flowing from West to East, bringing cool, nutrient-rich waters to the eastern Pacific beneath the eastern Pacific Warm Pool (EPWP) (Philander, 1980; Beltran et al., 2014). Consequently, the thermocline gradually becomes shallower towards the East, resulting in a contrast in sea surface temperature (SST) and thermocline depth (50–150 m) along the Equator. The upwelled waters contain essential nutrients like nitrate and phosphate, fostering the growth of phytoplankton and supporting a productive marine ecosystem in the region (Loubere, 2000).

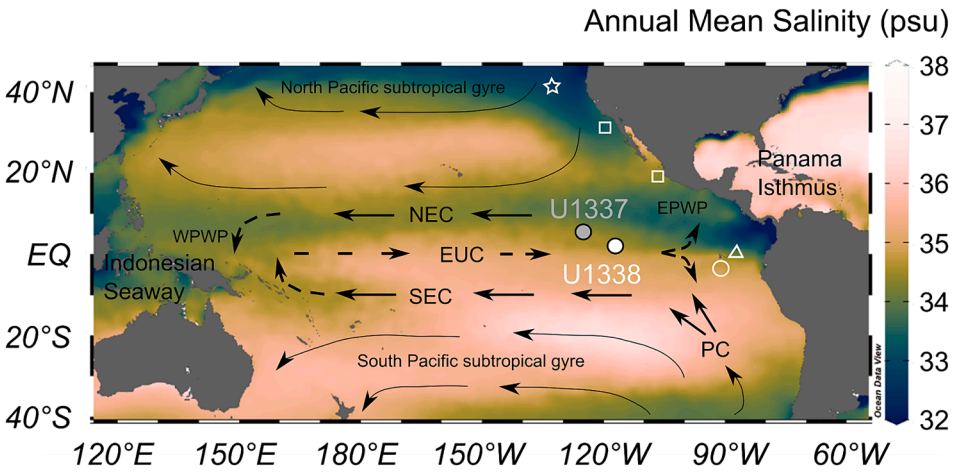

Fig. 1. Modern sea surface salinity data from Zweng et al. (2018) using a scientific colour map from Crameri (2023) showing the sediment core location of this study U1338 and the neighbouring core site U1337 drilled in the east equatorial Pacific. The star marks station "Gyre" of Wolfshorndl et al. (2019) and the two squares mark station 4–12 and 4–8 of Wolhowe et al. (2015), with reported hydrogen isotopes of alkenones from suspended particulate matter. The triangle marks the sediment core ODP Site 1240, with reported hydrogen isotopes of alkenones covering the Pleistocene (Quiros-Callazos 2020). The circle marks the sediment core ODP Site 846 with temperature, oxygen and carbon isotope records (Liu and Herbert, 2004; Lawrence et al., 2006; Herbert et al., 2016). (WPWP, Western Pacific Warm Pool; EPWP, Eastern Pacific Warm Pool; NEC, North Equatorial Current; SEC, South Equatorial Current; EUC, Equatorial Under Current; NECC, North Equatorial Counter Current, PC, Peru Current (modified after Pisias et al. (1995).

2.2. Sediments and age model

The sediment of Site U1338 Hole B (cores 3H–38H) is rich in well-preserved biogenic material, primarily consisting of nannofossil ooze with varying amounts of diatoms, radiolarians, and foraminifera (Pälike et al., 2010). The core, spanning 400 m, covers the middle Miocene to the Pleistocene, with predominant calcareous nannofossil assemblages (20 %–90 % $CaCO_3$ content). The age model for the U1338 record was determined using shipboard biostratigraphic (nannofossils, foraminifers, diatoms and radiolarians) and paleomagnetic dating (Pälike et al., 2010). The average sedimentation rate is ca. 27 m/Ma (Rousselle et al., 2013). For this study 44 sediment samples close to and between the sediment samples of the published $\delta^{18}O_{liths}$ data record from Rousselle et al. (2013) were ordered from IODP. We interpolated the age between the published age-depth points from Rousselle et al. (2013) for these 44 samples. The average time resolution for compound specific stable isotope analyses is 0.33 Myrs and for sea surface temperature estimations 0.09 Myrs.

2.3. Long-chain alkenones

Approximately 12 g of freeze-dried sediment was homogenized and 25 samples were extracted using accelerated solvent extraction (ASE 350 system, Dionex) using DCM/MeOH (9:1, v:v), while 19 samples were extracted by ultrasonic extraction using DCM/MeOH (2:1, v:v). The extract was dried using a Turbovap and the last remaining water, if present, was removed over a sodium sulfate ($NaSO_4$) column and separated into three fractions, apolar, ketone and polar, over an activated aluminum oxide Al_2O_3 column using hexane/DCM (9:1, v:v), hexane/DCM (1:1, v:v) and DCM/MeOH (1:1, v:v), respectively.

The ketone fractions were used for hydrogen and carbon isotope ratio analysis of alkenones after being measured using a gas chromatograph coupled to a flame ionisation detector (GC-FID), equipped with a CP Sil-5 fused silica capillary column (50 m × 0.32 mm, 0.12 μm thickness), to determine complexity of the fraction and the correct concentration of the alkenones. Furthermore, the GC-FID data was used to determine the $U^{K'}_{37}$ index and extend the SST record published by Rousselle et al. (2013) and Beltran et al. (2019) for this core. The $U^{K'}_{37}$ index was calculated from the abundance of di- and tri-unsaturated C_{37} alkenones according to Prahl and Wakeham (1987) (Eq. (1)) and converted into SST with the calibration published by Conte et al. (2006) (Eq. (2)).

$$U^{K'}_{37} = [C_{37:2}]/([C_{37:2}] + [C_{37:3}]) \quad (1)$$

$$SST = -0.957 + 54.293 \times U^{K'}_{37} - 52.894 \times (U^{K'}_{37})^2 + 28.321\,(U^{K'}_{37})^3 \quad (2)$$

Hydrogen isotope ratios of alkenones were measured in duplicate using a gas chromatograph coupled to a Thermo Delta V isotope ratio mass spectrometer (irMS) via high-temperature conversion reactor (Isolink I) and Conflo IV. The GC was equipped with an RTX-200 60 m column according to Weiss et al. (2019). We report the δ^2H ratio of the $C_{37:2}$ alkenone ($\delta^2H_{C37:2}$) determined by manual peak integration. The $C_{37:2}$ is the main alkenone peak, while $C_{37:3}$ and C_{38} peaks are present but in low relative abundance and most of the time below minimal intensity for the isotope ratio integration. The H^{3+} factor was determined daily before running samples and the day to day variability was never more than 0.5 ppm/nA. The performance and stability of the machine was monitored by measuring an *n*-alkane standard, Mix B5 (supplied by Arndt Schimmelmann, Indiana University). Samples were only run when the average difference and standard deviation between online and certified values was less than 5 ‰. To monitor the system performance squalene and C_{30} *n*-alkane were co-injected with each sample with measured values of −158 ± 6 ‰ and −65 ± 6 ‰, respectively. The offline determined values are −170 ± 4 ‰ for squalene and −79 ± 5 ‰ for C_{30} n-alkane, respectively.

For 37 (of 44) ketone fractions, the amount of alkenones left, after the δ^2H analysis, was high enough to analyse the stable carbon isotope composition. The ketone fractions were injected manually into a Thermo Trace 1310 GC equipped with an CP-Sil 5 (25 m × 0.32 mm; film thickness 0.12 mm) column, coupled to a Thermo Delta V irMS via a combustion reactor (Isolink II) and Conflo IV. The performance of the GC-irMS was tested using standards of per-deuterated C_{20} and C_{24} n-alkanes with measured values of −32.8 ± 0.2 ‰ and −27.1 ± 0.2 ‰, respectively, and co-injected with a daily GC standard to check chromatography. The offline determined values are −32.7 ‰ for C_{20} n-alkane and −27.0 ‰ for C_{24} n-alkanes, respectively. The GC-irMS Isolink II combustion reactor was oxidized for 15 min. at the start of every day, He backflushed for 10 min, and purged for 5 min. A shorter version, 2 min oxidation, 2 min He backflush and 2 min purge conditioning line, was conducted after every analytical run.

2.4. Calculation of seawater isotopes

For the calculation of the hydrogen isotopic composition of surface seawater (δ^2H_{SSW}) from hydrogen isotopes of $C_{37:2}$ we applied the open-ocean relationship determined based on surface ocean suspended particulate organic material (SPOM) by Gould et al. (2019) (Eq. (3)).

$$\delta^2H_{C37:2} = 1.48(\pm 0.4) \times \delta^2H_{SSW} - 199(\pm 3) \quad (3)$$

The oxygen isotopic composition of surface seawater ($\delta^{18}O_{SSW}$) was calculated by Rousselle et al. (2013), using the oxygen isotope ratios of coccolith calcite ($\delta^{18}O_{liths}$) and corrected with alkenone-derived SST according to Dudley et al. (1986) (Eq. (4)). The oxygen isotope ratios of $\delta^{18}O_{liths}$ were derived from the 2–5 μm fractions where the calcareous nannofossils are concentrated with an estimated purity of 75 % *Neoblaerhabdaceae* species.

$$SST = 21.7 - 5(\delta^{18}O_{liths} - \delta^{18}O_{SSW}) \quad (4)$$

We translated the $\delta^{18}O_{SSW}$ values into hydrogen isotopes of surface seawater with the modern open-ocean waterline reported by Hättig et al. (2023) (Eq. (5)).

$$\delta^2H_{SSW} = 6.58(\pm 0.07) \times \delta^{18}O_{SSW} - 0.12(\pm 0.03) \quad (5)$$

3. Results and discussion

3.1. Reconstruction of surface seawater isotopes based on δ^2H of alkenones

The compound-specific hydrogen isotope ratios of the $C_{37:2}$ alkenone range between approximately −220 ‰ to −260 ‰. Between 14.5–4 Ma a somewhat decreasing trend can be observed in this record, but most noticeably there are relatively rapid (<100–600 kyrs) and large variations of up 40 ‰ throughout the record (Fig. 2). This is in strong contrast to the reconstructed $\delta^{18}O_{SSW}$ record of Rousselle et al. (2013), which also shows a slight decreasing trend $\delta^{18}O_{SSW}$ values between 14–2.5 Ma but does not show the large variability observed in the $\delta^2H_{C37:2}$ record (Fig. S1, 2). Translating the $\delta^2H_{C37:2}$ record to δ^2H_{SSW} using the calibration of Gould et al. (2019) reveals also a slightly decreasing trend from −28 ‰ to −36 ‰ and relatively rapid variations of up to 23 ‰.

The reconstructed δ^2H_{SSW} values of −42 ‰ to −12 ‰ are strikingly more negative than the modern surface seawater δ^2H values which range typically between −5‰ and 10 ‰ in the open-ocean (Rohling et al., 2007; Hättig et al., 2023 Supplement) as well as reconstructed Miocene and Holocene δ^2H_{SSW} values reported for the Atlantic and Pacific (Hättig et al., 2023, 2024a). In contrast, the $\delta^{18}O_{SSW}$ range of −0.4 ‰ to 1.5 ‰ reconstructed by Rouselle et al. (2013) for site U1338 is comparable with the modern seawater isotope range (e.g., Rohling, 2007) and reconstructed bottom seawater isotopes of the Miocene Tasmanian Sea and North Atlantic (Hou et al., 2023, Hättig et al., 2024a). In

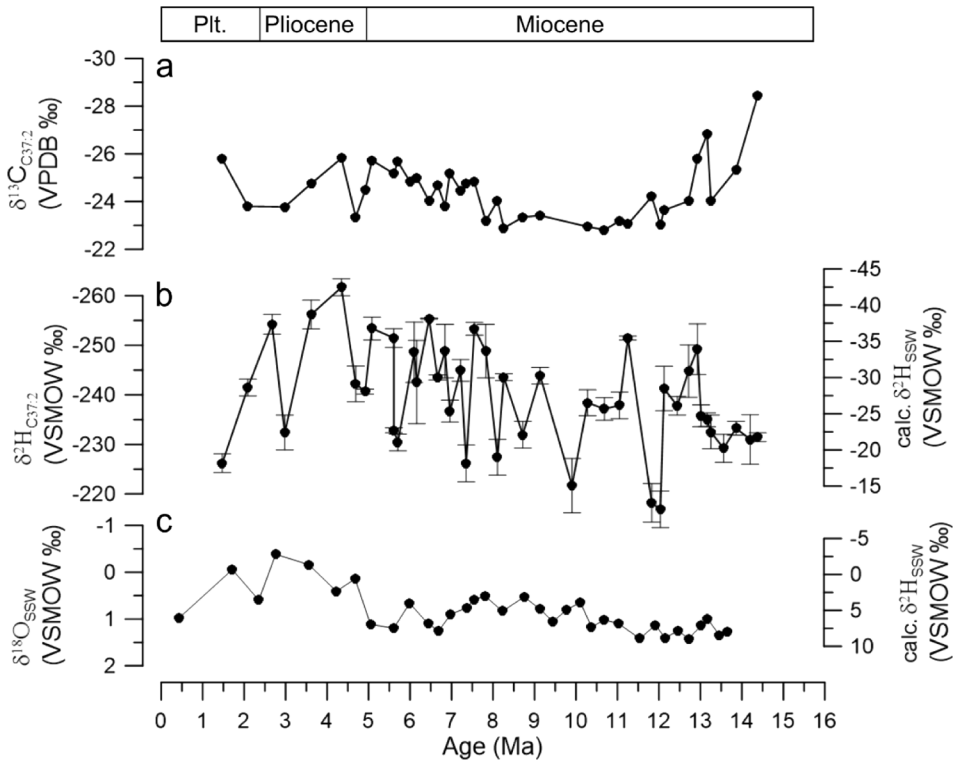

Fig. 2. Surface seawater isotope reconstructions for the Middle Miocene to Pleistocene eastern Equatorial Pacific site U1338. (a) Stable carbon isotopes of alkenones (b) Hydrogen isotopes of alkenones and calculated hydrogen isotopes of seawater (Eq. (3), Gould et al., 2019). The error bars represent the standard deviation of duplicate isotope measurements. (c) Oxygen isotopes of seawater based on oxygen isotopes of coccoliths (Rousselle et al., 2013), hydrogen isotopes of seawater calculated with the modern open-ocean waterline (Eq. (5), Hättig et al., 2023).

fact, when we convert the $\delta^{18}O_{SSW}$ of Rouselle et al. (2013) into $\delta^{2}H_{SSW}$ values (Fig. 2) using the modern open-ocean waterline (Eq. (5)), we calculate values much more positive than reconstructed using $\delta^{2}H_{C37:2}$ and in line with modern day $\delta^{2}H$ of surface waters in the Pacific (Wolfshorndl et al., 2019; Fig. 1). Thus, it seems likely that the reconstructed $\delta^{2}H_{SSW}$ values based on long-chain alkenones are unrealistic, i.e., they are too depleted in ^{2}H and unusually variable. Indeed, $\delta^{2}H_{C37}$ in modern day suspended particulate matter and surface sediments typically vary between ca. −170 ‰ – −210 ‰ (Gould et al., 2019; Mitsunaga et al., 2022) and studies from the southeastern Pacific Ocean, South Atlantic and Indian Ocean report Holocene $\delta^{2}H_{C37}$ values between −167 ‰ – −205 ‰ (Kasper et al., 2014, 2015; Simon et al., 2015; Petrick et al., 2015; Weiss et al., 2019; Hättig et al., 2023) and −180 ‰ – −220 ‰ for the Panama Basin in the equatorial eastern Pacific (Pahnke et al., 2007). Furthermore, Hättig et al. (2024a) reports Middle Miocene $\delta^{2}H_{C37:2}$ values of −174 ‰ – −200 ‰ for the North Atlantic Ocean. These values are all more enriched in ^{2}H compared to those measured in our record for site U1338. Only for the equatorial Pacific ODP site 1240 (Fig. 1), similarly depleted $\delta^{2}H_{C37:2}$ values of −220 ‰ – −245 ‰, were reported for the Pleistocene (Quirós-Collazos et al., 2020).

Even more remarkable, is the large and relatively rapid variability not reflected in the oxygen isotope record of coccoliths, which is not expected as both proxies should reflect the isotopic composition of surface seawater. It is highly unlikely that the $\delta^{2}H_{SSW}$ changed so strongly due to climatic or oceanographic changes while at the same time these factors would not affect $\delta^{18}O_{SSW}$. Therefore, we suspect that the hydrogen isotopic composition of alkenones at U1338 is impacted by factors affecting the isotopic fractionation during biosynthesis of alkenones.

3.2. Impact of ecology on $\delta^{2}H$ of alkenones

One cause for the large ^{2}H-depletion and high variability observed for the $\delta^{2}H_{C37}$ may be changes in haptophyte species as isotopic fractionation strongly depends on species. For example, coastal or brackish water Group II haptophytes fractionate substantially less at the same salinity than the open-ocean Group III haptophytes (M'Boule et al., 2014). Beltran et al. (2014) observed for sediment core U1338 a dominance of small *Dictyococcites* spp. in the calcareous nannofossil abundance with no major changes observed in the assemblages. *Dictyococcites/Reticulofenestra* are ancestors of *G. oceanica* and *E. huxleyi* (Marlowe et al., 1990; Young et al., 1992; Henderiks and Pagani, 2008). Culture studies have reported that the modern open-ocean species *G. oceanica* and *E. huxleyi* fractionate differently compared to each other, i.e., *G. oceanica* synthesized alkenones were ~30 ‰ more depleted in ^{2}H compared to *E. huxleyi* under similar growing conditions in Schouten et al. (2006). Thus, variations in species may account for some of the variability, although assemblages are relatively constant and it is therefore likely that variations in species does not account for the overall strong depletion in ^{2}H. Furthermore, there is no evidence in the alkenone distributions that would suggest significant species changes such as varying abundance of C_{38} methyl alkenones. Group III marine haptophytes have typically high abundance of C_{38} methyl alkenones while Group II brackish haptophytes do not produce them (or only traces) (Zheng et al., 2019; Kaiser et al., 2019). Thus, it seems unlikely that the large depletion in ^{2}H and rapid changes in $\delta^{2}H_{C37:2}$ can be fully explained by species variability.

Other factors which are known to impact $\delta^{2}H$ fractionation in cultures are growth rate (Schouten et al., 2006; Sachse et al., 2012; Sachs and Kawka, 2015) and light (Wolhowe et al., 2009, 2015; van der Meer et al., 2015; Weiss et al., 2017). Interestingly, Wolfshorndl et al. (2019) observed increasing depletion in $\delta^{2}H$ of C_{37} alkenones with depth on the order of 10 ‰–30 ‰ in the euphotic zone in the North Pacific, despite constant salinity and $\delta^{2}H$ of seawater. This large change was attributed to decreasing irradiance and/or nutrient limited growth rates with increasing water depth. Wolhowe et al. (2015) observed $\delta^{2}H_{C37}$ ratios

between −190 ‰ down to −245 ‰ in suspended material from the Gulf of California and eastern tropical North Pacific, with δ^2H_{C37} decreasing with depth and light availability. Thus, both studies observed depleted and highly variable hydrogen isotopes of alkenones produced between 10–70 m water depth in the modern Pacific Ocean.

To investigate this, we analyzed the stable carbon isotopic composition of alkenones ($\delta^{13}C_{C37:2}$) which is impacted by CO_2 concentration, cell geometry and growth rate (e.g., Jasper and Hayes, 1990; Bidigare et al., 1997; Popp et al., 1998; Riebesell et al., 2000; Benthien et al., 2002; Laws et al., 2002). Since cell geometry can be assumed to be relatively constant during this period, $\delta^{13}C_{C37:2}$ should mainly reflect changes in pCO_2 and growth rate. Indeed, this approach has been used before to evaluate the quality of the hydrogen isotope data, identify outliers and constrain the impact of growth rate (Wolhowe et al., 2015; Gould et al., 2019; Wolfshorndl et al., 2019; Mitsunaga et al., 2022). The $\delta^{13}C_{C37:2}$ measured in sediment core U1338 range between −22 ‰ and −28 ‰. At ~16 Ma $\delta^{13}C_{C37:2}$ is −28 ‰ and increases till ~11 Ma up to −23 ‰. Between 8 Ma and 4 Ma $\delta^{13}C_{C37:2}$ decreases again from −23 ‰ to −26 ‰ (Fig. S1). Interestingly, the large changes in $\delta^2H_{C37:2}$ alkenones are not observed in $\delta^{13}C_{C37:2}$ as would be expected if both are predominantly impacted by growth rate. This implies that growth rate is unlikely to explain the large variability and depletion in ^2H observed in our alkenone record.

Thus, the most likely factor which could explain the large variability and depletion in ^2H in our record is light limitation due to subsurface production of alkenones. Van der Meer et al. (2015) have shown that during the production of alkenones at high light conditions, i.e., at photosynthetic active radiation (PAR) > 200 μmol·photons·m^{-2}·s^{-1}, experienced in surface waters (Frouin and Murakami, 2007), fractionation tends to be relatively constant and independent on the level of irradiance (van der Meer et al., 2015). However, below 200 μmol·photons·m^{-2}·s^{-1} a strong increase in isotopic fractionation during biosynthesis of alkenones is observed leading to depletions of > 40 ‰. Furthermore, this depletion in ^2H is depending on the level of irradiance, i.e., a lower PAR results in increasing fractionation and depletion in ^2H of the alkenones. Thus, if alkenones are produced in subsurface waters at light conditions well below 200 μmol·photons·m^{-2}·s^{-1}, as is the case for the Pacific (PAR < 50 μmol·photons·m^{-2}·s^{-1}; Wolhowe et al., 2014, 2015), then it will lead to a strong depletion in ^2H as well as large changes with relatively small changes in light intensity. Therefore, both the large depletion in ^2H as well as the large variability of 40 ‰ in the $\delta^2H_{C37:2}$ record of U1338 may be explained by a substantial contribution of alkenones produced at subsurface water depth under low light conditions. This may be specific for the equatorial Pacific Ocean as light penetrates deeply into subsurface waters which are relatively rich in nutrients, thereby stimulating subsurface production of alkenones (Popp et al., 2006; Wolhowe et al., 2015; Wolfshorndl et al., 2019). Indeed, it may explain the results of Quiros-Callazos et al. (2020) for ODP site 1240, also in the equatorial Pacific, where strongly depleted $\delta^2H_{C37:2}$ values, between of −220 ‰ – −245 ‰, were found for Pleistocene sediments. Our results suggests that in these particular regions, where there is large subsurface production of alkenones, it might not be possible to use the hydrogen isotopic composition of C_{37} alkenones as a proxy for δ^2H_{SSW}.

4. Conclusion

We observed relatively negative and highly variable hydrogen isotope ratios of $C_{37:2}$ alkenones throughout the middle Miocene-Pliocene sediment record of eastern equatorial Pacific IODP site U1338. Although the long-term trend is similar to the previously published $\delta^{18}O_{SSW}$ reconstructions based on coccoliths, derived from the same group of organisms, the hydrogen isotope record of alkenones does not seem to primarily reflect changes in the surface seawater isotopes. Comparison with modern Pacific Ocean data and analysis of $\delta^{13}C_{C37:2}$ suggest that subsurface production of alkenones at low light intensity had a strong impact on the hydrogen isotopic composition of alkenones. Care should be taken to use δ^2H of alkenones in regions where subsurface production of alkenones might take place.

CRediT authorship contribution statement

Katrin Hättig: Writing – review & editing, Writing – original draft, Visualization, Methodology, Investigation, Formal analysis, Data curation, Conceptualization. **Panteleimon Prokopiou:** Writing – review & editing, Methodology, Data curation. **Stefan Schouten:** Writing – review & editing, Supervision, Project administration, Investigation, Conceptualization, Funding acquisition. **Marcel T.J. van der Meer:** Writing – review & editing, Visualization, Supervision, Project administration, Methodology, Conceptualization.

Declaration of competing interest

The authors declare that they have no known competing financial interests or personal relationships that could have appeared to influence the work reported in this paper.

Data availability

All data can be found in the Supplementary Information. Data is also available at PANGAEA (https://doi.org/10.1594/PANGAEA.968585, Hättig et al., 2024b). All processed sediment samples are stored at NIOZ, i.e., TLE, apolar, ketone, polar fractions of U1338.

Acknowledgments

We thank Michelle Penkrot from IODP Gulf Coast Repository for providing samples of U1338. Jort Ossebaar and Ronald van Bommel are thanked for analytical support. We would like to thank the Associate Editor and reviewers for taking the time and effort necessary to review the manuscript and for their useful comments on this manuscript. This work was carried out under the umbrella of the Netherlands Earth System Science Centre (NESSC). This project has received funding from the European Union's Horizon 2020 research and innovation programme under the Marie Sklodowska-Curie, grant agreement No 847504.

Appendix A. Supplementary data

Supplementary data to this article can be found online at https://doi.org/10.1016/j.orggeochem.2024.104840.

References

Beltran, C., De Rafé Lis, M., Minoletti, F., Renard, M., Sicre, M.A., Ezat, U., 2007. Coccolith $\delta^{18}O$ and alkenone records in middle Pliocene orbitally controlled deposits: high-frequency temperature and salinity variations of sea surface water. Geochemistry, Geophysics, Geosystems 8, Q05003.

Beltran, C., Rouselle, G., Backman, J., Wade, B.S., Sicre, M.A., 2014. Miocene in the eastern equatorial Pacific. Paleoceanography 29, 210–222.

Beltran, C., Rousselle, G., de Rafélis, M., Sicre, M.A., Labourdette, N., Schouten, S., 2019. Evolution of the zonal gradients across the equatorial Pacific during the Miocene-Pleistocene. Journal of Sedimentary Research 89, 242–252.

Benthien, A., Andersen, N., Schulte, S., Müller, P.J., Schneider, R.R., Wefer, G., 2002. Carbon isotopic composition of the $C_{37:2}$ alkenone in core top sediments of the South Atlantic Ocean: effects of CO_2 and nutrient concentrations. Global Biogeochemical Cycles 16, 1012.

Bidigare, R., Fluegge, A., Freeman, K.H., Hanson, K.L., Hayes, J.M., Hollander, D., Jasper, J.P., King, L.L., Laws, L.E., Milder, J., Millero, F.J., Pancost, R., Popp, B.N., Steinberg, P.A., Wakeham, S.G., 1997. Consistent fractionation of ^{13}C in nature and in the laboratory: growth-rate effects in some haptophyte algae. Global Biogeochemical Cyles 11, 279–292.

Cannariato, K.G., Ravelo, A.C., 1997. Pliocene-Pleistocene evolution of eastern tropical Pacific surface water circulation and thermocline depth. Paleoceanography 12, 805–820.

Chivall, D., M'Boule, D., Sinke-Schoen, D., Sinninghe Damsté, J.S., Schouten, S., van der Meer, M.T.J., 2014. The effects of growth phase and salinity on the hydrogen

isotopic composition of alkenones produced by coastal haptophyte algae. Geochimica et Cosmochimica Acta 140, 381–390.
[dataset] Crameri, F., 2023. Scientific colour maps (8.0.0), Zenodo, https://doi.org/10.5281/zenodo.5501399.
de Leeuw, J.W., van der Meer, F.W., Rijpstra, W.I.C., Schenck, P.A., 1980. On the occurrence and structural identification of long chain unsaturated ketones and hydrocarbons in sediments. In: Douglas, A.G., Maxwell, J.R. (Eds.), Advances in Organic Geochemistry 1979. Oxford Pergamon Press, pp. 211–217.
Dudley, W.C., Blackwelder, P., Brand, L., Duplessy, J.-C., 1986. Stable isotopic composition of coccoliths. Marine Micropaleontology 1–8.
Flower, B.P., Kennett, J.P., 1994. The middle Miocene climatic transition: East Antarctic ice sheet development, deep ocean circulation and global carbon cycling. Palaeogeography, Palaeoclimatology, Palaeoecology 108, 537–555.
Frouin, R., Murakami, H., 2007. Estimating photosynthetically available radiation at the ocean surface from ADEOS-II global imager data. Journal of Oceanography 63, 493–503.
Gould, J., Kienast, M., Dowd, M., Schefuß, E., 2019. An open-ocean assessment of alkenone δD as a paleo-salinity proxy. Geochimica et Cosmochimica Acta 246, 478–497.
Hättig, K., Schouten, S., Louwye, S., van der Meer, M.T.J., 2024a. Stable Middle Miocene seawater isotopes in the eastern North Atlantic Ocean. ESS Open Archive.
[dataset] Hättig, K., Schouten, S., Louwye, S., van der Meer, M.T.J. 2024b. Sea surface temperature and stable isotopes of alkenones for IODP Site 321 U1338. PANGAEA, https://doi.org/10.1594/PANGAEA.968585.
Hättig, K., Varma, D., Schouten, S., van der Meer, M.T.J., 2023. Glacial-interglacial seawater isotope change near the Chilean Margin as reflected by δ^2H values of C_{37} alkenones. Climate of the Past 19, 1919–1930.
Haug, G.H., Tiedemann, R., 1998. Effect of the formation of the Isthmus of Panama on Atlantic Ocean thermohaline circulation. Nature 393, 673–676.
Haug, G.H., Tiedemann, R., Zahn, R., Ravelo, A.C., 2001. Role of Panama uplift on oceanic freshwater balance. Geology 29, 207–210.
Henderiks, J., Pagani, M., 2008. Coccolithophore cell size and the Paleogene decline in atmospheric CO_2. Earth Planetary Science Letters 269, 576–584.
Herbert, T.D., Lawrence, K.T., Tzanova, A., Peterson, L.C., Caballero-Gill, R., Kelly, C.S., 2016. Late Miocene global cooling and the rise of modern ecosystems. Nature Geoscience 9, 843–847.
Holbourn, A., Kuhnt, W., Kochhann, K.G.D., Andersen, N., Sebastian Meier, K.J., 2015. Global perturbation of the carbon cycle at the onset of the Miocene Climatic Optimum. Geology 43, 123–126.
Hou, S., Stap, L.B., Paul, R., Nelissen, M., Hoem, F.S., Ziegler, M., Sluijs, A., Sangiorgi, F., Bijl, P.K., 2023. Reconciling Southern Ocean fronts equatorward migration with minor Antarctic ice volume change during Miocene cooling. Nature Communications 14, 7230.
Jasper, J.P., Hayes, J.M., 1990. A carbon isotope record of CO_2 levels during the late Quaternary. Nature 347, 462–464.
Kamikuri, S., Motoyama, I., Nishi, H., Iwai, M., 2009. Evolution of Eastern Pacific Warm Pool and upwelling processes since the middle Miocene based on analysis of radiolarian assemblages: response to Indonesian and Central American Seaways. Palaeogeography, Palaeoclimatology, Palaeoecology 280, 469–479.
Kasper, S., van der Meer, M.T.J., Mets, A., Zahn, R., Sinninghe Damsté, J.S., Schouten, S., 2014. Salinity changes in the Agulhas leakage area recorded by stable hydrogen isotopes of C_{37} alkenones during Termination I and II. Climate of the Past 10, 251–260.
Kasper, S., van der Meer, M.T.J., Castañeda, I.S., Tjallingii, R., Brummer, G.J.A., Sinninghe Damsté, J.S., Schouten, S., 2015. Testing the alkenone D/H ratio as a paleo indicator of sea surface salinity in a coastal ocean margin (Mozambique Channel). Organic Geochemistry 78, 62–68.
Lawrence, K.T., Liu, Z., Herbert, T.D., 2006. Evolution of the Eastern Tropical Pacific Through Plio-Pleistocene Glaciation. Science 312, 79–83.
Laws, E.A., Popp, B.N., Cassar, N., Tanimoto, J., 2002. ^{13}C discrimination patterns in oceanic phytoplankton: likely influence of CO_2 concentrating mechanisms, and implications for palaeoreconstructions. Functional Plant Biology 29, 323–333.
Lear, C.H., Elderfield, H., Wilson, P.A., 2000. Cenozoic deep-sea temperatures and global ice volumes from Mg/Ca in benthic foraminiferal calcite. Science 80, 269–272.
Leduc, G., Sachs, J.P., Kawka, O.E., Schneider, R.R., 2013. Holocene changes in eastern equatorial Atlantic salinity as estimated by water isotopologues. Earth and Planetary Science Letters 362, 151–162.
Liu, Z., Herbert, T.O., 2004. High-latitude influence on the eastern equatorial Pacific climate in the early Pleistocene epoch. Nature 427, 720–723.
Loubere, P., 2000. Marine control of biological production in the eastern equatorial Pacific Ocean. Nature 406, 497–500.
M'Boule, D., Chivall, D., Sinke-Schoen, D., Sinninghe Damsté, J.S., Schouten, S., van der Meer, M.T.J., 2014. Salinity dependent hydrogen isotope fractionation in alkenones produced by coastal and open ocean haptophyte algae. Geochimica et Cosmochimica Acta 130, 126–135.
Marlowe, I.T., Brassell, S.C., Eglinton, G., Green, J.C., 1990. Long-chain alkenones and alkyl alkenoates and the fossil coccolith record of marine sediments. Chemical Geology 88, 349–375.
Mitsunaga, B.A., Novak, J., Zhao, X., Dillon, J.A., Huang, Y., Herbert, T.D., 2022. Alkenone δ^2H values – a viable seawater isotope proxy? New core-top $\delta^2H_{C37:3}$ and $\delta^2H_{C37:2}$ data suggest inter-alkenone and alkenone-water hydrogen isotope fractionation are independent of temperature and salinity. Geochimica et Cosmochimica Acta 339, 139–156.
Mudelsee, M., Raymo, M.E., 2005. Slow dynamics of the Northern Hemisphere glaciation. Paleoceanography 20.
Pahnke, K., Sachs, J.P., Keigwin, L., Timmermann, A., Xie, S.P., 2007. Eastern tropical Pacific hydrologic changes during the past 27,000 years from D/H ratios in alkenones. Paleoceanography 22, PA4214.
Pälike, H., Lyle, M., Nishi, H., Raffi, I., Gamage, K., Klaus, A., Scientists, Expedition 320/321 Scientists, 2010. Proceedings of the IODP, vol. 320/321, Integrated Ocean Drill. Program Manage. Int., Inc., Tokyo.
Pälike, H., Nishi, H., Lyle, M., Raffi, I., Klaus, A., Gamage, K., Expedition 320/321 Scientists, 2009. Pacific Equatorial Transect. IODP Preliminary Report 320.
Petrick, B.F., McClymont, E.L., Marret, F., van der Meer, M.T.J., 2015. Changing surface water conditions for the last 500ka in the Southeast Atlantic: implications for variable influences of Agulhas leakage and Benguela upwelling. Paleoceanography 30, 1153–1167.
Philander, S.G.H., 1980. The Equatorial Undercurrent revisited. Annual Review of Earth and Planetary Sciences 8, 191–204.
Pisias, N.G., Mayer, L.A., Mix, A.C., 1995. Paleoceanography of the Eastern equatorial pacific during the Neogene: synthesis of leg 138 drilling results. Proceedings of the Ocean Drilling Program, Scientific Results 138.
Popp, B.N., Laws, E.A., Bidigare, R.R., Dore, J.E., Hanson, K.L., Wakeham, S.G., 1998. Effect of phytoplankton cell geometry on carbon isotopic fractionation. Geochimica et Cosmochimica Acta 62, 69–77.
Popp, B.N., Prahl, F.G., Wallsgrove, R.J., Tanimoto, J., 2006. Seasonal patterns of alkenone production in the subtropical oligotrophic North Pacific. Paleoceanography 21, PA1004.
Quirós-Collazos, L., Calvo, E., Schouten, S., van der Meer, M.T.J., Rodrigo-Gámiz, M., Pena, L.D., Cacho, I., Pelejero, C., 2020. Controls on primary productivity in the Eastern Equatorial Pacific, East of the Galapagos Islands, during the penultimate deglaciation. Paleoceanography and Paleoclimatology 35, 1–18.
Riebesell, U., Revill, A.T., Holdsworth, D.G., Volkman, J.K., 2000. The effects of varying CO_2 concentration on lipid composition and carbon isotope fractionation in Emiliania huxleyi. Geochimica et Cosmochimica Acta 64, 4179–4192.
Rohling, E.J., 2007. Progress in paleosalinity: Overview and presentation of a new approach. Paleoceanography 22, 1–9.
Rousselle, G., Beltran, C., Sicre, M.A., Raffi, I., de Rafélis, M., 2013. Changes in sea-surface conditions in the Equatorial Pacific during the middle Miocene-Pliocene as inferred from coccolith geochemistry. Earth and Planetary Science Letters 361, 412–421.
Sachs, J.P., Kawka, O.E., 2015. The influence of growth rate on $^2H/^1H$ fractionation in continuous cultures of the coccolithophorid Emiliania huxleyi and the diatom Thalassiosira pseudonana. PLoS One 10, e0141643.
Sachs, J.P., Maloney, A.E., Gregersen, J., Paschall, C., 2016. Effect of salinity on $^2H/^1H$ fractionation in lipids from continuous cultures of the coccolithophorid Emiliania huxleyi. Geochimica et Cosmochimica Acta 189, 96–109.
Sachs, J.P., Maloney, A.E., Gregersen, J., 2017. Effect of light on $^2H/^1H$ fractionation in lipids from continuous cultures of the diatom Thalassiosira pseudonana. Geochimica et Cosmochimica Acta 209, 204–215.
Sachse, D., Billault, I., Bowen, G.J., Chikaraishi, Y., Dawson, T.E., Feakins, S.J., Freeman, K.H., Magill, C.R., McInerney, F.A., van der Meer, M.T.J., Polissar, P., Robins, R.J., Sachs, J.P., Schmidt, H.L., Sessions, A.L., White, J.W.C., West, J.B., Kahmen, A., 2012. Molecular paleohydrology: interpreting the hydrogen-isotopic composition of lipid biomarkers from photosynthesizing organisms. Annual Review of Earth and Planetary Sciences 40, 221–249.
Savin, S.M., Douglas, R., Stehli, F.G., 1975. Tertiary marine paleotemperatures. Bulletin of the Geological Society of America 86, 1499–1510.
Schouten, S., Ossebaar, J., Schreiber, K., Kienhuis, M.V.M., Langer, G., Bijma, J., 2006. The effect of temperature and salinity on the stable hydrogen isotopic composition of long chain alkenones produced by Emiliania huxleyi and Gephyrocapsa oceanica. Biogeosciences 3, 113–119.
Shackleton, N.J., 1974. Attainment of isotopic equilibrium between ocean water and the benthonic foraminifera geuns Uvigerina: isotopic changes in the ocean during the last glacial. Colloques Internationaux du CNRS 219, 203–210.
Simon, M.H., Gong, X., Hall, I.R., Ziegler, M., Barker, S., Knorr, G., van der Meer, M.T.J., Kasper, S., Schouten, S., 2015. Salt exchange in the Indian-Atlantic Ocean Gateway since the Last Glacial Maximum: a compensating effect between Agulhas Current changes and salinity variations? Paleoceanography 30, 1318–1327.
Srinivasan, M.S., Sinha, D.K., 2000. Ocean circulation in the tropical Indo-Pacific during early Pliocene (5.6-4.2 Ma): Paleobiogeographic and isotopic evidence. Journal of Earth System Science 109, 315–328.
Steph, S., Tiedemann, R., Prange, M., Groeneveld, J., Nürnberg, D., Reuning, L., Schulz, M., Haug, G.H., 2006. Changes in Caribbean surface hydrography during the Pliocene shoaling of the Central American Seaway. Paleoceanography 21, 1–25.
Tian, J., Yang, M., Lyle, M.W., Wilkens, R., Shackford, J.K., 2013. Obliquity and long eccentricity pacing of the Middle Miocene climate transition. Geochemistry, Geophysics, Geosystems 14, 1740–1755.
Tian, J., Ma, W., Lyle, M.W., Shackford, J.K., 2014. Synchronous mid-Miocene upper and deep oceanic $\delta^{13}C$ changes in the east equatorial Pacific linked to ocean cooling and ice sheet expansion. Earth and Planetary Science Letters 406, 72–80.
Tian, J., Ma, X., Zhou, J., Jiang, X., Lyle, M., Shackford, J., Wilkens, R., 2018. Paleoceanography of the east equatorial Pacific over the past 16 Myr and Pacific-Atlantic comparison: high resolution benthic foraminiferal $\delta^{18}O$ and $\delta^{13}C$ records at IODP Site U1337. Earth and Planetary Science Letters 499, 185–196.
van der Meer, M.T.J., Baas, M., Rijpstra, W.I.C., Marino, G., Rohling, E.J., Sinninghe Damsté, J., Schouten, S., 2007. Hydrogen isotopic compositions of long-chain alkenones record freshwater flooding of the Eastern Mediterranean at the onset of sapropel deposition. Earth and Planetary Science Letters 262, 594–600.
van der Meer, M.T.J., Benthien, A., French, K.L., Epping, E., Zondervan, I., Reichart, G.J., Bijma, J., Sinninghe Damsté, J.S., Schouten, S., 2015. Large effect of irradiance on

hydrogen isotope fractionation of alkenones in Emiliania huxleyi. Geochimica et Cosmochimica Acta 160, 16–24.
Volkman, J.K., Eglinton, G., Corner, E.D.S., Sargent, J.R., 1980. Novel unsaturated straight-chain C_{37} C_{39} methyl and ethyl ketones in marine sediments and a coccolithophore Emiliania huxleyi. Physics and Chemistry of the Earth 12, 219–227.
Weiss, G.M., de Bar, M.W., Stolwijk, D.J., Schouten, S., Sinninghe Damsté, J.S., van der Meer, M.T.J., 2019. Paleosensitivity of hydrogen isotope ratios of long-chain alkenones to salinity changes at the Chile Margin. Paleoceanography and Paleoclimatology 34, 978–989.
Weiss, M.G., Pfannerstill, Y.E., Schouten, S., Sinninghe Damsté, S.J., van der Meer, M.T.J., 2017. Effects of alkalinity and salinity at low and high light intensity on hydrogen isotope fractionation of long-chain alkenones produced by Emiliania huxleyi. Biogeosciences 14, 5693–5704.
Wolfshorndl, M., Danford, R., Sachs, J.P., 2019. $^{2}H/^{1}H$ fractionation in microalgal lipids from the North Pacific Ocean: growth rate and irradiance effects. Geochimica et Cosmochimica Acta 246, 317–338.
Wolhowe, M.D., Prahl, F.G., Probert, I., Maldonado, M., 2009. Growth phase dependent hydrogen isotopic fractionation in alkenone-producing haptophytes. Biogeosciences 6, 1681–1694.
Wolhowe, M.D., Prahl, F.G., Langer, G., Oviedo, A.M., Ziveri, P., 2015. Alkenone δD as an ecological indicator: a culture and field study of physiologically-controlled chemical and hydrogen-isotopic variation in C_{37} alkenones. Geochimica et Cosmochimica Acta 162, 166–182.
Young, J.R., Didymus, J.M., Brown, P.R., Prins, B., Mann, S., 1992. Crystal assembly and phylogenetic evolution in heterococcoliths. Nature 356, 516–518.
[dataset] Zweng, M.M., Reagan, J.R., Seidov, D., Boyer, T.P., Locarnini, R.A., Garcia, H. E., Mishonov, A.V., Baranova, O.K., Weathers, K., Paver, C.R., Smolyar, I., 2018. World Ocean Atlas 2018, Volume 2: Salinity. A. Mishonov Technical Ed.; NOAA Atlas NESDIS 82, pp. 50, World Ocean Atlas 2018, 82, pp. 50.